Nuclear Engineering and Technology 55 (2023) 2256–2262

Contents lists available at ScienceDirect

Nuclear Engineering and Technology

journal homepage: www.elsevier.com/locate/net

Original Article

# High-temperature electrochemical corrosion behavior of SA106 Grade B carbon steel with corrosion inhibitors in HyBRID solution

Sung-Wook Kim*, Sang-Yoon Park, Chang-Hyun Roh, Sun-Byeong Kim

*Korea Atomic Energy Research Institute, Republic of Korea*

ARTICLE INFO

*Article history:*
Received 23 September 2022
Received in revised form
8 February 2023
Accepted 5 March 2023
Available online 7 March 2023

*Keywords:*
Hydrazine-based reductive metal ion decontamination (HyBRID)
Carbon steel
Corrosion inhibitor
Electrochemistry
Potentiodynamic polarization

ABSTRACT

The electrochemical corrosion behaviors of SA106 Grade B (SA106B) carbon steel in $H_2SO_4$-$N_2H_4$ and $H_2SO_4$-$N_2H_4$-$CuSO_4$ solutions at 95 °C have been investigated with the addition of commercial corrosion inhibitors (CI#30 and No. 570S), to determine the stability of SA106B in the hydrazine-based reductive metal ion decontamination (HyBRID) process. The potentiodynamic polarization experiment revealed that the corrosion inhibitors were capable of lowering the corrosion rate of SA106B in $H_2SO_4$-$N_2H_4$ solution. It was found that the corrosion inhibitors induced formation of fixed surface layer on the carbon steel upon the corrosion. This corrosion inhibition performance was reduced in the presence of $CuSO_4$ in the solution owing to the chemical reactions between organic compounds in the corrosion inhibitors and $CuSO_4$. CI#30 showed a better corrosion inhibition effect in the $H_2SO_4$-$N_2H_4$-$CuSO_4$ solution. Although the corrosion inhibitors can provide better stability to SA106B in the HyBRID solution, their application should be carefully considered because it may result in reduced decontamination performance and increased secondary waste generation.



## 1. Introduction

Various chemical decontamination techniques, such as hydrazine ($N_2H_4$)-based reductive metal ion decontamination (HyBRID), have been developed to reduce the radioactivity of coolant loop systems in nuclear power plants [1–3]. Oxide layers (e.g., $Fe_3O_4$) usually grow on the inner surface of the loop system because structural materials (generally metallic compounds) are exposed to high-temperature water (coolant) under high pressure. Following the oxide layer growth, dangerous radioactive isotopes (RIs) (e.g., $^{60}Co$) dissolved in high-temperature water are incorporated into the oxide layers, resulting in the accumulation of radioactivity. Thereafter, RIs must be removed properly by chemical decontamination before dismantling the loop system to guarantee employee safety and prevent the spread of RIs. The HyBRID process utilizes a $H_2SO_4$-based solution as a decontamination medium in the presence of $N_2H_4$ and $CuSO_4$ to convert the solid-state oxide layers into water-soluble ionic forms, as described in reactions (1) and (2), with an example of the dissociation of $Fe_3O_4$ to $Fe^{2+}$ ion [2,3].

$$N_2H_5^+(aq) + 4Cu^{2+}(aq) \rightarrow 5H^+(aq) + 4Cu^+(aq) + N_2(g), \quad (1)$$

$$Fe_3O_4(s) + 8H^+(aq) + 2Cu^+(aq) \rightarrow 3Fe^{2+}(aq) + 2Cu^{2+}(aq) + 4H_2O(l), \quad (2)$$

Following the destruction of the oxide layer by chemical reaction, the RIs incorporated in the oxide layers are removed from the inner surface of the loop system. The clean inner surface of the structural materials of the loop system is expected to be exposed after decontamination.

In contrast, corrosion of structural materials has emerged as an issue associated with chemical decontamination because of the highly corrosive nature of the decontamination solutions (e.g., $H_2SO_4$ in the HyBRID process) [2–5]. After the removal of RI-contaminated oxide layers, the clean surface of the structural material is susceptible to chemical degradation by the decontamination solution. This becomes more critical in a pressurized heavy water reactor (PHWR) system, because key components (e.g., feeder pipe) of its coolant loop system are made of corrosion-prone carbon steel (e.g., SA106 Grade B (SA106B)) [6]. Structural material corrosion generates additional water-soluble metal ions from the loop system during chemical decontamination. Eventually, this increases the amount of final waste generated in the system, which is strongly related to the concentration of metal ions in the

* Corresponding author. Korea Atomic Energy Research Institute, 989-111 Daedeok-daero, Yuseong-gu, Daejeon, 34057, Republic of Korea.
*E-mail address:* swkim818@kaeri.re.kr (S.-W. Kim).

https://doi.org/10.1016/j.net.2023.03.008

decontamination solution. Generation of large amounts of final waste increases the process burden and cost involved in the back-end process of chemical decontamination. In this respect, investigating the corrosion behavior of structural material is essential for designing an efficient decontamination process.

Electrochemistry has been widely used to study the corrosion behavior of metallic compounds [7–9]. In our previous studies, the room-temperature electrochemical corrosion behaviors of the structural materials were investigated in HyBRID solution [4,5]. It was revealed that the introduction of corrosion inhibitors could restrict the room-temperature corrosion of SA106B [5]. For instance, the corrosion current ($I_{corr}$) of SA106B in the $H_2SO_4$-$N_2H_4$ solution was reduced to ~1/5 of the original by adding CI#30, a commercialized corrosion inhibitor [5].

The operating temperature of the HyBRID process is typically 95 °C, which is essential for obtaining sufficient decontamination efficiency [2,3]. Nevertheless, previous electrochemical studies were performed at room temperature; therefore, it is thought that the results obtained from room-temperature electrochemical experiments cannot reflect the actual process condition [4,5]. In this respect, the high-temperature (95 °C) electrochemical corrosion behavior of SA106B was investigated in this study. The effect of commercial corrosion inhibitors (CI#30 and No. 570S in $H_2SO_4$-$N_2H_4$ solution with and without $CuSO_4$) on the corrosion property of SA106B was investigated using the potentiodynamic polarization technique.

## 2. Material and methods

$H_2SO_4$ (Daejung Chemicals & Metals, 98%), $N_2H_4$•$H_2O$ (Junsei Chemical, 98%), and $CuSO_4$•$5H_2O$ (Sigma Aldrich, 98%) were used to prepare the HyBRID solution, which was used as an electrolyte. CI#30 (Hangil Industries Chemical) and No. 570S (Asahi Chemical) were chosen as the corrosion inhibitors. Table 1 lists the components of these corrosion inhibitors.

An electrochemical cell with a three-electrode configuration was constructed for the potentiodynamic polarization experiments. A double-walled jacketed glass vessel was used as reactor. Hot water was circulated in the outer jacket to maintain the temperature of the electrolyte at 95 °C. The electrolyte (1 L) was composed of 0.05 M $H_2SO_4$ and 0.095 M $N_2H_4$ with and without 0.5 mM $CuSO_4$. An SA106B disk, installed inside a Teflon-lined electrode kit with an electrode opening area of 1 $cm^2$, was used as the working electrode. The SA106B disk was polished using SiC paper (up to 2000 grit size) before assembling the electrode kit. A coiled Pt wire (diameter = 0.5 mm, Alfa Aesar) was used as a counter electrode. An Ag/AgCl electrode (Fisherbrand, Accumet 13-620-223A) was used as the reference electrode. The potentiodynamic experiment was conducted using a potentiostat (Biologic, SP-150). The potential range was varied from −0.4 to +0.4 V versus open-circuit potential of the working electrode with a scan rate of 0.02 V $s^{-1}$. Corrosion inhibitors were gradually added (up to 5.0 mL) to the electrolyte during the electrochemical investigation. The corrosion parameters, such as $I_{corr}$, corrosion potential ($E_{corr}$), and Tafel constants for anodic ($\beta_a$) and cathodic ($\beta_c$) reactions were extracted by Tafel extrapolation. The inhibition efficiency (IE) was defined using the following equation:

$$IE\ (\%) = (1 - I_{corr}/I^0_{corr}) \times 100, \quad (3)$$

where $I^0corr$ represents $I_{corr}$ value without the corrosion inhibitors.

The chemical stability of the corrosion inhibitors against $CuSO_4$ was examined by adding 5 mL of CI#30 or No. 570S in 0.05 M $H_2SO_4$ solution (500 mL) containing $CuSO_4$ (0.01 M). The mixed solution was then heated to 60 °C for 3 h. After the reaction, the solution was vacuum-filtered (pore size = 2–4 μm, F2142, CHMLAB) to recover the precipitates.

An SA106B coupon (15 mm × 25 mm × 3.5 mm with a 4 mm-diameter hole) immersion test was performed to reveal its surface property after corrosion. The base solution (500 mL) comprised of 0.05M $H_2SO_4$ and 0.095M $N_2H_4$ with and without 0.5 mM $CuSO_4$. The corrosion inhibitors, CI#30 and No. 570S, were added to each base solution at a concentration of 0.6 mL $L^{-1}$. The test coupons were immersed in the test solution at 95 °C for 24 h to sufficiently grow surface corrosion products. The recovered test coupon was cleaned using water and wet wipers.

Energy-dispersive X-ray spectroscopy (EDS) (Horiba, X-MAX) operated by scanning electron microscopy (Hitachi, SU-8010) was used to identify the chemical components of the reaction products. The crystal structure of the reaction products were analyzed by X-ray diffraction (XRD) (Bruker, D8 Advance).

**Table 1**
Chemical components in commercial corrosion inhibitors, CI#30 and No. 570S.

| Product name | Chemical | Composition (%) |
|---|---|---|
| CI#30 | Triethanolamine lauryl sulfate | 30 |
| | Lauryl betaine | 10 |
| | Water | Balance |
| No. 570S | 2-Propanol | < 0.5 |
| | 2-Aminoethanol | 2.0 |
| | Quaternary ammonium salt (confidential) | 1–5 |
| | Nonionic surfactant (confidential) | 1–5 |
| | Organic sulfur compound (confidential) | 1–5 |
| | Water | Balance |

## 3. Results and discussion

Figs. 1 and 2 depict the potentiodynamic polarization curves of SA106B in $H_2SO_4$-$N_2H_4$ solution at 95 °C with the addition of CI#30 and No. 570S, respectively. The curves tend to move to the upper left side with the addition of the corrosion inhibitor, suggesting $I_{corr}$ reduction of SA106B. The electrochemical parameters extracted from Figs. 1 and 2 are listed in Tables 2 and 3, respectively. $I_{corr}$, which is directly related to the corrosion rate, decreased with the addition of the corrosion inhibitors. This demonstrates that both

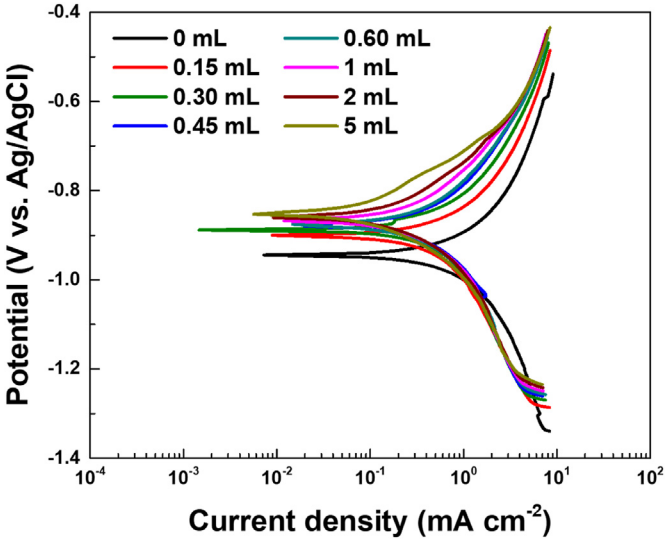


**Fig. 1.** Potentiodynamic polarization curves of SA106B in $H_2SO_4$-$N_2H_4$ solution after the addition of CI#30 at 95 °C.

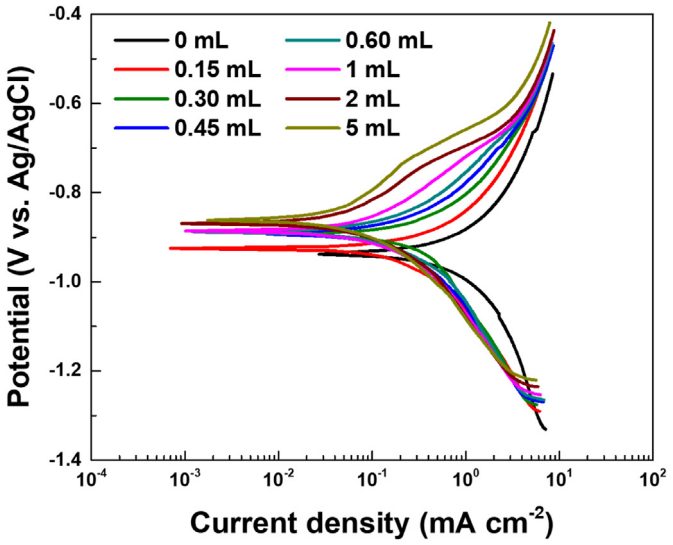


**Fig. 2.** Potentiodynamic polarization curves of SA106B in $H_2SO_4$-$N_2H_4$ solution after addition of No. 570S at 95 °C.

CI#30 and No. 570S could effectively reduce the corrosion rate of SA106 in $H_2SO_4$-$N_2H_4$ solution at high temperatures. Fig. 3 compares the effect of adding different corrosion inhibitors on the $I_{corr}$ values. In both cases, $I_{corr}$ tended to drastically decrease in the initial stage of addition and was gradually saturated as the input amount increased. The $I_{corr}$ reduction in the saturation region was more than 80% for CI#30 and 90% for No. 570S (see IE values in Tables 2 and 3); therefore, No. 570S displayed better corrosion inhibition efficiency in $H_2SO_4$-$N_2H_4$ solution at 95 °C.

$CuSO_4$ is a key component of the HyBRID solution because $Cu^{+/2+}$ redox cycling enhances the dissolution rate of the oxide layers, as described in reactions (1) and (2) [2,3]. Thus, an additional electrochemical investigation of SA106B was performed in $H_2SO_4$-$N_2H_4$-$CuSO_4$ solution, as shown in Fig. 4 and Table 4 for CI#30 and in Fig. 5 and Table 5 for No. 570S. For comparison, the results (Figs. 4 and 5) are overlaid in Fig. 3. A noticeable change in the polarization curves in the CI#30 case was observed, following the addition of > 1 mL corrosion inhibitors, as shown in Fig. 4. This implies that a small amount of CI#30 cannot suppress SA106B corrosion in $H_2SO_4$-$N_2H_4$-$CuSO_4$ solution at 95 °C. For No. 570S, as shown in Fig. 5, the polarization curves shifted when the input amount reached 5 mL, suggesting that a large amount of No. 570S is required to protect the surface of SA106B in $H_2SO_4$-$N_2H_4$-$CuSO_4$ solution at 95 °C. Therefore, it is evident that $CuSO_4$ in the solution disturbs the corrosion inhibition effect of both CI#30 and No. 570S, and more corrosion inhibitor is needed to protect SA106B when $CuSO_4$ is present in the HyBRID solution. In contrast to the $H_2SO_4$-$N_2H_4$ solution, CI#30 performed better in $H_2SO_4$-$N_2H_4$-$CuSO_4$ solution, implying less disturbance of CI#30 by $CuSO_4$. The saturated $I_{corr}$ reduction in $H_2SO_4$-$N_2H_4$-$CuSO_4$ solution was in the range of 70–80% in CI#30, which is lower than that in the $H_2SO_4$-$N_2H_4$ solution. In the case of No. 570S, $I_{corr}$ reduction (~80%) was observed with an input amount of 5 mL, the maximum amount in the experimental condition.

To rationalize the negative effect of $CuSO_4$ on the corrosion inhibitors, chemical stability tests of CI#30 and No. 570S in $H_2SO_4$ solution in the presence of $CuSO_4$ were conducted, as shown in Fig. 6. The CI#30-containing test solution was transparent (Fig. 6a) immediately after preparation at room temperature, whereas brown precipitates were found in the No. 570S-containing solution (Fig. 6d). This implies that a chemical reaction between No. 570S and $CuSO_4$ occurred even at room temperature. As the temperature was increased to 60 °C, the CI#30-containing solution became opaque with the formation of fine precipitates (Fig. 6b), and more precipitates were formed in the No. 570S-containing solution (Fig. 6e). Both the solutions were vacuum-filtered to recover the precipitate. As shown in Fig. 6c and f, the amount of precipitate formed in No. 570S was much larger than that of the CI#30, indicating a greater vulnerability of No. 570S against $CuSO_4$ insertion. The EDS analysis in Fig. 6g reveals that Cu, S, and O (also potentially with C) comprised the precipitate recovered from the No. 570S-containing solution. The precipitate was amorphous as shown in Fig. 6h. It is speculated that the organic compounds in CI#30 and No. 570S (Table 1) formed precipitates of water-insoluble metal-organic complexes with Cu and S ions in the solution. Therefore, as shown in Fig. 3, the corrosion inhibitors showed no corrosion

**Table 2**
Electrochemical parameters obtained from potentiodynamic polarization of SA106B in $H_2SO_4$-$N_2H_4$ solution after the addition of CI#30 at 95 °C.

| Amount (mL) | $I_{corr}$ (μA) | IE (%) | $E_{corr}$ (mV vs. Ag/AgCl) | $\beta_a$ (mV dec$^{-1}$) | $\beta_c$ (mV dec$^{-1}$) | $R_p$ (kΩ) |
|---|---|---|---|---|---|---|
| 0 | 669.4 | - | -944.0 | 212.8 | 237.8 | 0.073 |
| 0.15 | 373.4 | 44.2 | -901.7 | 152.2 | 228.6 | 0.106 |
| 0.30 | 324.7 | 51.5 | -888.3 | 169.7 | 192.0 | 0.121 |
| 0.45 | 311.5 | 53.5 | -879.3 | 183.8 | 185.5 | 0.129 |
| 0.60 | 247.6 | 63.0 | -877.6 | 159.5 | 163.9 | 0.142 |
| 1 | 215.9 | 67.7 | -867.2 | 168.6 | 159.8 | 0.165 |
| 2 | 131.2 | 80.4 | -860.2 | 136.3 | 114.0 | 0.206 |
| 5 | 107.6 | 83.9 | -852.2 | 145.5 | 131.1 | 0.279 |

**Table 3**
Electrochemical parameters obtained from potentiodynamic polarization of SA106B in $H_2SO_4$-$N_2H_4$ solution after the addition of No. 570S at 95 °C.

| Amount (mL) | $I_{corr}$ (μA) | IE (%) | $E_{corr}$ (mV vs. Ag/AgCl) | $\beta_a$ (mV dec$^{-1}$) | $\beta_c$ (mV dec$^{-1}$) | $R_p$ (kΩ) |
|---|---|---|---|---|---|---|
| 0 | 688.3 | - | -938.7 | 231.8 | 245.5 | 0.075 |
| 0.15 | 283.8 | 58.8 | -924.9 | 156.2 | 243.6 | 0.146 |
| 0.30 | 248.2 | 63.9 | -891.4 | 143.4 | 228.7 | 0.154 |
| 0.45 | 218.8 | 68.2 | -891.4 | 175.0 | 241.7 | 0.202 |
| 0.60 | 96.9 | 85.9 | -887.2 | 111.4 | 119.2 | 0.259 |
| 1 | 77.6 | 88.7 | -885.0 | 145.6 | 121.7 | 0.371 |
| 2 | 49.6 | 92.8 | -870.3 | 152.2 | 102.2 | 0.536 |
| 5 | 42.4 | 93.8 | -861.3 | 171.9 | 108.9 | 0.684 |

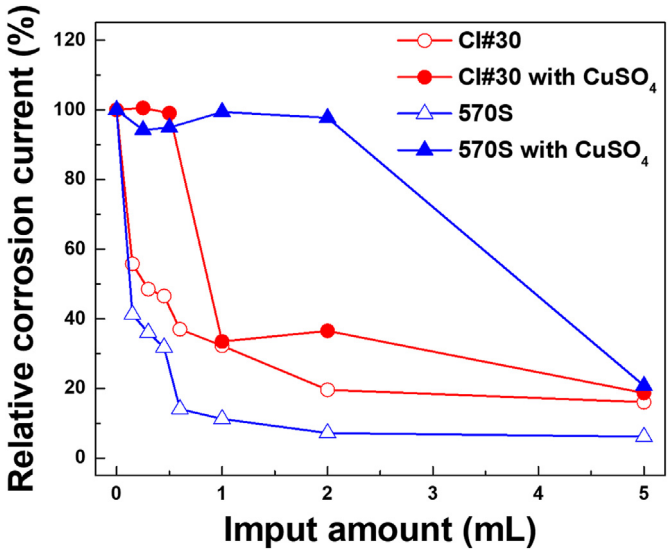


**Fig. 3.** Relative $I_{corr}$ of SA106B in $H_2SO_4$-$N_2H_4$ and $H_2SO_4$-$N_2H_4$-$CuSO_4$ solutions after the addition of CI#30 or No. 570S.

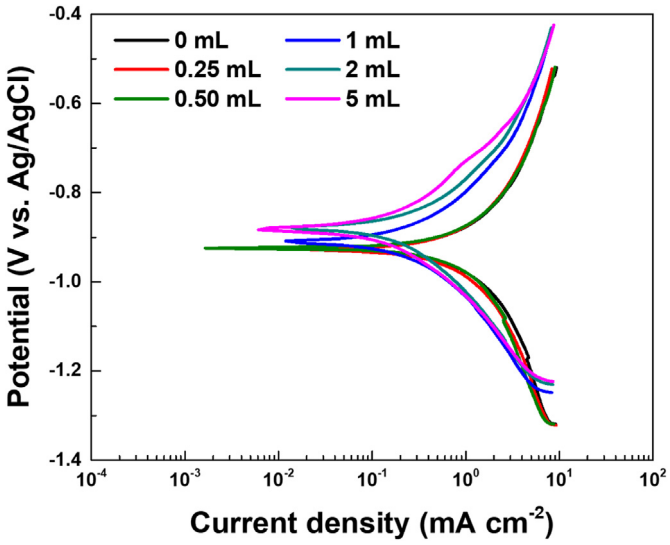


**Fig. 4.** Potentiodynamic polarization curves of SA106B in $H_2SO_4$-$N_2H_4$-$CuSO_4$ solution after addition of CI#30 at 95 °C.

inhibition effect in the low-concentration region, where the organic compounds were consumed by $CuSO_4$. It seems that the organic compounds in No. 570S are more likely to capture the Cu ions in the solution, and thus, the disturbance becomes more significant in the No. 570S case.

It is considered that the corrosion products of the carbon steel are predominantly dissolved in acidic test solutions in an ionic state

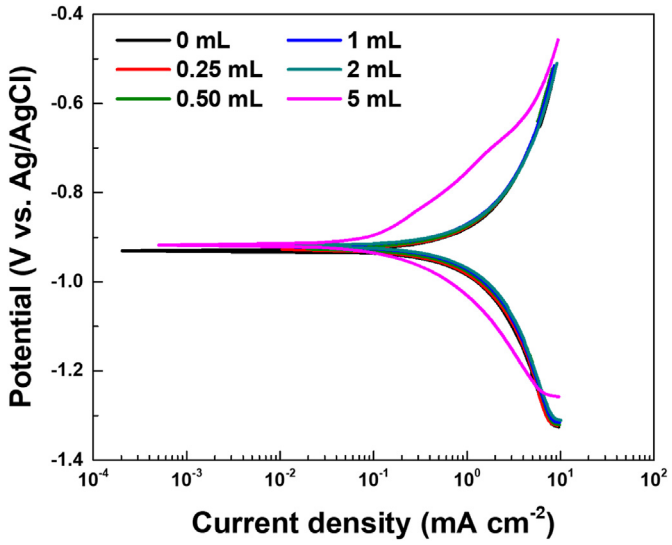


**Fig. 5.** Potentiodynamic polarization curves of SA106B in $H_2SO_4$-$N_2H_4$-$CuSO_4$ solution after the addition of No. 570S at 95 °C.

because $Fe^{2+}$ is energetically stable in the HyBRID solution [2,3]. However, a small amount of corrosion products was also found on the surface of the carbon steel. To reveal the surface state of SA106B after the corrosion, the carbon steel coupons were immersed in the test solutions at 95 °C for 24 h to reveal the surface corrosion products, as shown in Fig. 7. Fig. 7a shows that the surface of the test coupons immediately after recovery was covered with black particulates, whose dominant component is thought to be $Fe_3O_4$. After surface cleaning, the metallic surface was exposed in $H_2SO_4$-$N_2H_4$ (Fig. 7b) and $H_2SO_4$-$N_2H_4$-$CuSO_4$ (Fig. 7e) cases, suggesting that the surface products were not strongly attached to SA106B when the inhibitors were not present. In contrary, a tightly fixed surface layer was observed with the addition of the corrosion inhibitors in $H_2SO_4$-$N_2H_4$ solution (Fig. 7c and d). This means that the chemical components of the corrosion inhibitors stabilize the surface layer during corrosion. The EDS results in Fig. 8 reveal the existence of O and Fe in the fixed layer, whereas the peak intensity of O in the metallic surface was quite low, indicating that the fixed layer was an oxide (or hydroxide) phase of Fe. Cu may also play a role in the formation of the surface layer when $CuSO_4$ existed (Fig. 8c). The fixed layer, however, was not uniform and fully covered the carbon steel surface. Thus the SA106B surface was expected to be exposed to the corrosive environment. The fixed layer was removed partially (Fig. 7f) or almost completely (Fig. 7g) in the presence of $CuSO_4$. It is thought that the corrosion inhibitor consumption by $CuSO_4$ hindered the fixed layer formation or render the fixed layer unstable, resulting in the increased corrosion rate, as identified in the electrochemical investigation. Fig. 8d shows the XRD patterns of the test coupons. The peak intensity of metallic Fe was greatly reduced when the fixed layer existed, but additional peak evolution was not identified. This implies that the

**Table 4**
Electrochemical parameters obtained from potentiodynamic polarization of SA106B in $H_2SO_4$-$N_2H_4$-$CuSO_4$ solution after the addition of CI#30 at 95 °C.

| Amount (mL) | $I_{corr}$ (μA) | IE (%) | $E_{corr}$ (mV vs. Ag/AgCl) | $\beta_a$ (mV $dec^{-1}$) | $\beta_c$ (mV $dec^{-1}$) | $R_p$ (kΩ) |
|---|---|---|---|---|---|---|
| 0 | 668.8 | - | -927.4 | 209.9 | 217.9 | 0.070 |
| 0.25 | 672.3 | -0.52 | -925.7 | 215.1 | 259.8 | 0.076 |
| 0.50 | 662.4 | 0.95 | -924.3 | 203.4 | 239.4 | 0.072 |
| 1 | 223.9 | 66.5 | -909.4 | 170.1 | 189.9 | 0.174 |
| 2 | 244.4 | 63.5 | -878.7 | 178.3 | 235.1 | 0.180 |
| 5 | 124.9 | 81.3 | -884.1 | 158.2 | 156.7 | 0.274 |

**Table 5**
Electrochemical parameters obtained from potentiodynamic polarization of SA106B in $H_2SO_4$-$N_2H_4$-$CuSO_4$ solution after the addition of No. 570S at 95 °C.

| Amount (mL) | $I_{corr}$ (μA) | IE (%) | $E_{corr}$ (mV vs. Ag/AgCl) | $\beta_a$ (mV $dec^{-1}$) | $\beta_c$ (mV $dec^{-1}$) | $R_p$ (kΩ) |
|---|---|---|---|---|---|---|
| 0 | 674.3 | - | -930.5 | 213.7 | 233.0 | 0.072 |
| 0.25 | 635.2 | 5.80 | -927.0 | 200.4 | 219.2 | 0.072 |
| 0.50 | 640.0 | 5.08 | -927.0 | 204.1 | 204.7 | 0.069 |
| 1 | 670.2 | 0.60 | -921.5 | 208.0 | 218.0 | 0.069 |
| 2 | 658.9 | 2.29 | -918.1 | 194.6 | 209.1 | 0.067 |
| 5 | 140.1 | 79.2 | -916.0 | 192.1 | 126.1 | 0.236 |

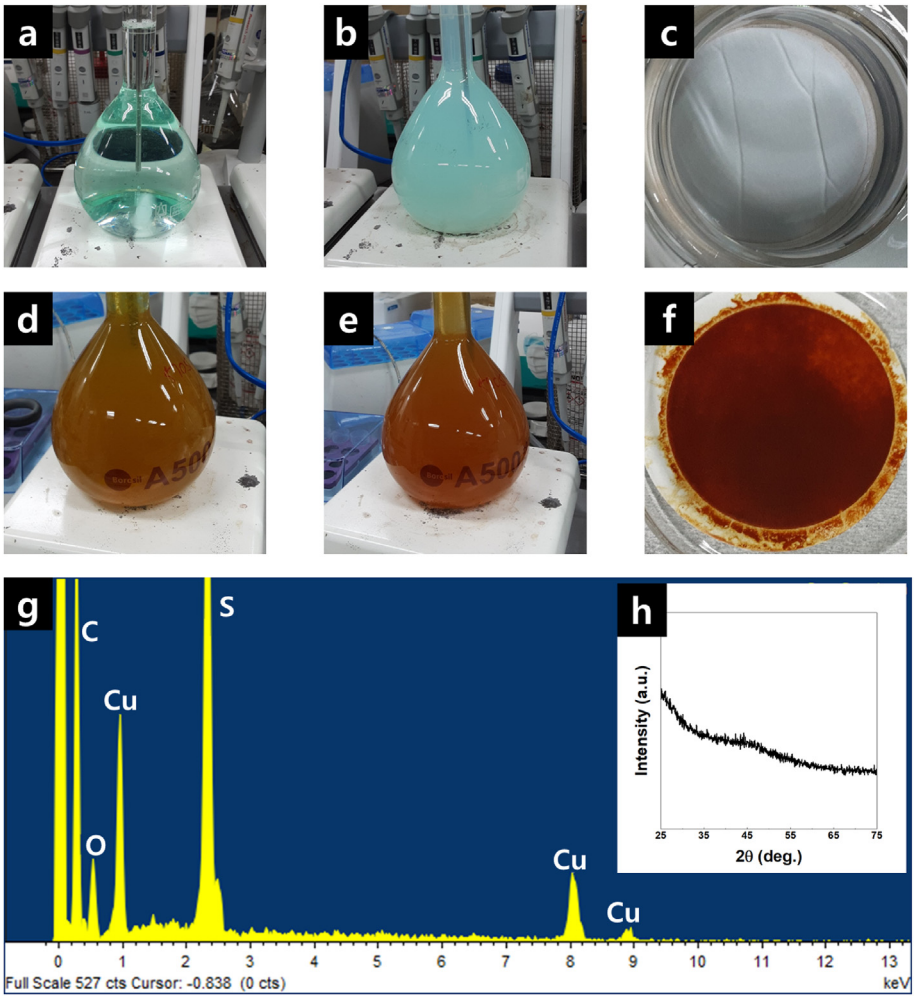


**Fig. 6.** Chemical stability test results of corrosion inhibitors with $CuSO_4$: (a) CI#30-containing solution at room temperature, (b) CI#30-containing solution at 60 °C, (c) precipitates recovered from CI#30-containing solution at 60 °C, (d) No. 570S-containing solution at room temperature, (e) No. 570S-containing solution at 60 °C, (f) precipitates recovered from No. 570S-containing solution at 60 °C, (g) EDS result of precipitates in Fig. 6f, and (h) XRD pattern of precipitates in Fig. 6f.

fixed layer is a poorly crystalline or amorphous phase composed of Fe and O (and H).

It was revealed that corrosion inhibitors CI#30 and No. 570S could reduce the corrosion rate of SA106B in the HyBRID solution at 95 °C. Corrosion protection is an important factor in the design of a chemical decontamination solution, particularly in the PHWR system, in which carbon steel is used to construct the coolant loop system [6]. Nevertheless, the utilization of corrosion inhibitors in the HyBRID process should be carefully determined for the following reasons:

- Cu ion consumption: It is well understood that the catalytic effect of Cu ions promotes the oxide removal reaction in the HyBRID process [2,3]. As shown in Fig. 6, the organic compounds in the corrosion inhibitors tend to consume Cu ions in solution to form solid-state phases. This means that the concentration of the Cu ions dissolved in the HyBRID solution decreased with the introduction of the corrosion inhibitors. The reduced Cu ion concentration may result in reduced oxide dissolution rate [2]. Subsequently, the overall decontamination performance could deteriorate with the addition of corrosion inhibitors to the HyBRID solution. The precipitates, formed by the chemical reaction between Cu ions and corrosion inhibitors, may float inside the decontamination solution during operation. If the precipitates are not properly treated during the operation, they may result in an overload or failure of the decontamination

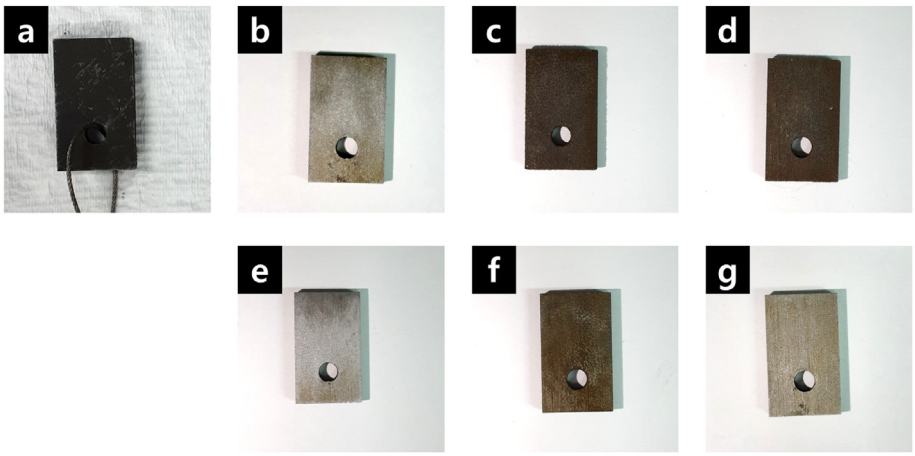


**Fig. 7.** SA106B coupons after immersion in various test solutions (a) just after recovery and (b–g) after surface cleaning: (b) $H_2SO_4$-$N_2H_4$ solution, (c) $H_2SO_4$-$N_2H_4$-Cl#30 solution, (d) $H_2SO_4$-$N_2H_4$-No. 570S solution, (e) $H_2SO_4$-$N_2H_4$-$CuSO_4$ solution, (f) $H_2SO_4$-$N_2H_4$-$CuSO_4$-Cl#30 solution, and (g) $H_2SO_4$-$N_2H_4$-$CuSO_4$-No. 570S solution.

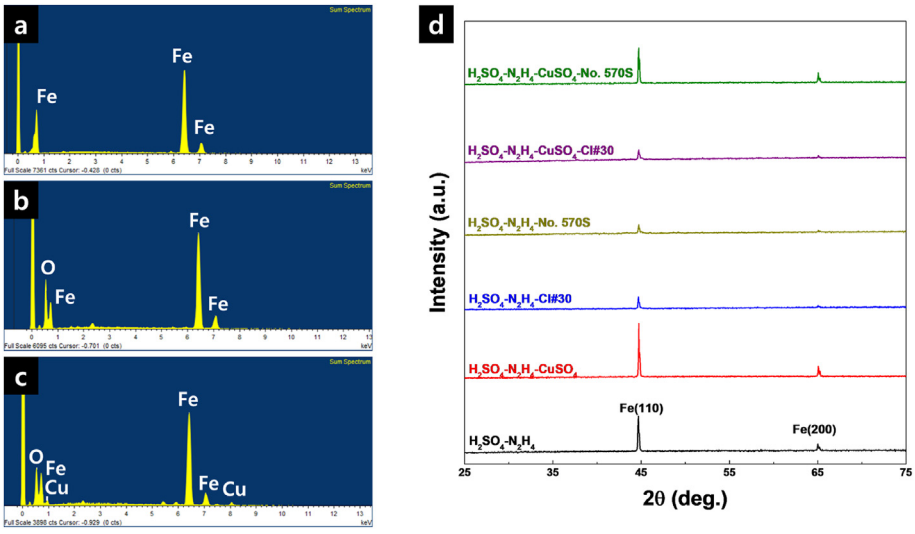


**Fig. 8.** (a–c) EDS analysis of SA106B coupons immersed in (a) $H_2SO_4$-$N_2H_4$ solution, (b) $H_2SO_4$-$N_2H_4$-Cl#30 solution, and (c) $H_2SO_4$-$N_2H_4$-$CuSO_4$-Cl#30 solution and (d) XRD analysis of SA106B coupons immersed in various test solutions.

solution circulation pumps because they could clog inside the moving parts of the pumps.

- Generation of organic compound-containing wastes: One of the main purposes of HyBRID process development is to avoid the use of organic compounds for the chemical decontamination of the loop system [2,3]. Conventional chemical decontamination processes use organic acids (e.g., oxalic acid, citric acids, etc.) as major components in the decontamination solutions; the HyBRID solution is composed of inorganic compounds ($H_2SO_4$, $N_2H_4$, and $CuSO_4$), without any organic additives. The HyBRID process is expected to generate less secondary waste than the conventional organic acid-based processes. It has been reported that the SP-HyBRID process (SP = sulfuric acid/permanganate) could achieve more than 60% waste reduction compared to the organic acid-based chemical decontamination process, called HP-CORD UV (HP = permanganic acid, CORD = chemical oxidation reduction decontamination, UV = ultraviolet) [10]. A significant amount of ion-exchange (IX) resins is required to treat the organic compounds in the waste solution generated during conventional decontamination processes [10]. In the HyBRID process, which is free from organic compounds, the waste solution is treated by an inorganic precipitation method; thus, usage of the IX resins can be minimized to decrease secondary waste generation [10]. Additionally, temporary storage and stabilization of radioactive organic wastes are challenging issues in terms of safe radioactive waste management [11]. When organic corrosion inhibitors are introduced into the HyBRID solution, an organic compound-containing waste solution is generated during the oxide layer decomposition; this problem needs to be resolved.

## 4. Conclusions

A high-temperature electrochemical potentiodynamic polarization experiment was carried out to investigate the corrosion behavior of SA106B in the HyBRID solution with corrosion inhibitors at a practical operating temperature (95 °C). The corrosion inhibitors Cl#30 and No. 570S effectively protected the surface of SA106B against corrosion in $H_2SO_4$-$N_2H_4$ solution. The corrosion inhibitors induced the formation of a surface layer that reduced the corrosion rate of SA106B. Nevertheless, the corrosion inhibition

performance of the corrosion inhibitors was degraded in the presence of $CuSO_4$ (an essential component of the HyBRID process), owing to the chemical reaction between Cu ions and organic compounds present in the corrosion inhibitors. No. 570S was found to be more reactive with $CuSO_4$ compared to that of CI#30 and it was evident that CI#30 exhibited better inhibition performance in the HyBRID solution containing $CuSO_4$. Despite the corrosion inhibition abilities of CI#30 and 570S, their utilization in the HyBRID process needs to be further investigated with consideration of their impact on the oxide removal chemistry by $CuSO_4$ consumption and secondary waste generation by organic compounds.

## Declaration of competing interest

The authors declare that they have no known competing financial interests or personal relationships that could have appeared to influence the work reported in this paper.

## Acknowledgements

This study was supported by a National Research Foundation of Korea (NRF) grant funded by the Korean government (MISP) (RS-2022-00155421).

## References

[1] C.J. Wood, A review of the application of chemical decontamination technology in the United States, Prog. Nucl. Energy 23 (1990) 35–80, https://doi.org/10.1016/0149-1970(90)90013-U.

[2] S. Kim, S. Park, W. Choi, H. Won, J. Park, B. Seo, Magnetite dissolution by copper catalyzed reductive decontamination, J. Nucl. Fuel Cycle Waste Technol. 16 (2018) 421–429, https://doi.org/10.7733/jnfcwt.2018.16.4.421.

[3] B.-C. Lee, S.-B. Kim, J.-K. Moon, S.-Y. Park, Evaluation of reaction spontaneity for acidic and reductive dissolutions of corrosion metal oxides using HyBRID chemical decontamination, J. Radioanal. Nucl. Chem. 323 (2020) 91–103, https://doi.org/10.1007/s10967-019-06962-3.

[4] S.-W. Kim, S.-Y. Park, C.-H. Roh, J.-H. Shim, S.-B. Kim, Electrochemical corrosion study on base metals used in nuclear power plant in the HyBRID process for chemical decontamination, Nucl. Eng. Technol. 54 (2022) 2329–2333, https://doi.org/10.1016/j.net.2021.12.008.

[5] S.-W. Kim, S.-Y. Park, C.-H. Roh, J.-H. Shim, S.-B. Kim, Effect of corrosion inhibitors on SA106 Grade B carbon steel in $H_2SO_4$-$N_2H_4$ solution for the hydrazine-based reductive ion decontamination process, Chem. Paper 76 (2022) 6517–6522, https://doi.org/10.1007/s11696-022-02338-2.

[6] A. Fillipovic, E.G. Price, D. Barber, J. Nickerson, Material and Fabrication Considerations for the CANDU-PHWR Heat Transport System, AECL-9421, International Conference of Nuclear Equipment-Welding and Q.A., Sarajevo, Yugoslavia, March 1987.

[7] E. McCafferty, Validation of corrosion rates measured by the Tafel extrapolation method, Corr. Sci. 47 (2005) 3202–3215, https://doi.org/10.1016/j.corsci.2005.05.046.

[8] X.L. Zhang, Z.H. Jiang, Z.P. Yao, Y. Song, Z.D. Wu, Effects of scan rate on the potentiodynamic polarization curve obtained to determine the Tafel slopes and corrosion current density, Corr. Sci. 51 (2009) 581–587, https://doi.org/10.1016/j.corsci.2008.12.005.

[9] V.K. Gattu, W.L. Ebert, J.E. Indacochea, T.A. Cruse, J.A. Forter, Electrochemical corrosion of multiphase stainless steel-based alloy nuclear waste forms, npj Mater. Degrad. 6 (2022) 14, https://doi.org/10.1038/s41529-022-00220-w.

[10] J.Y. Jung, H.C. Eun, S.Y. Park, J.S. Park, N.O. Chang, S.B. Kim, B.K. Seo, S.J. Park, A study on the removal of impurities in a SP-HyBRID decontamination wastewater of the primary coolant system in a pressurized water reactor, J. Radioanal. Nucl. Chem. 318 (2018) 1339–1345, 10/1007/s10967-018-6219-0.

[11] L.R. van Loon, W. Hummel, The Role of Organics on the Safety of a Radioactive Waste Repository, Paul Scherrer Institut Annual Report, 1993.